Evaluating the Relationship Between Powder Characteristics, Defects, and Final Build Properties for L-PBF WC–Co

P. Govender, D. Hagedorn-Hansen, D. C. Blaine, and N. Sacks

Abstract With rising interest in additive manufacturing (AM) techniques, there is increased focus on research that evaluates critical parameters that guide the selection of powders suitable for AM. This study focuses on two spray-dried WC–Co powders (12 and 17 wt% Co) and evaluates the relationship between typical powder characteristics, defects occurring post printing and the final build parameters. The precursor powders and parts produced using a laser powder bed fusion (L-PBF) process were characterized. Suitable WC–Co printing parameters were used for building cutting tool inserts. The as-built parts were analysed for density and defect formation due to printing. The final part properties were evaluated and related back to the precursor powder properties.

Keywords Tungsten carbide-cobalt · Powder characteristics · Laser powder bed fusion · cutting tools

P. Govender (✉) · D. C. Blaine
Department of Mechanical and Mechatronic Engineering, University of Stellenbosch, Stellenbosch, South Africa
e-mail: 18375391@sun.ac.za

D. C. Blaine
e-mail: dcblaine@sun.ac.za

P. Govender · D. Hagedorn-Hansen · D. C. Blaine · N. Sacks
DSI-NRF Centre of Excellence in Strong Materials, Johannesburg, South Africa
e-mail: devonh@sun.ac.za

N. Sacks
e-mail: natashasacks@sun.ac.za

D. Hagedorn-Hansen · N. Sacks
Department of Industrial Engineering, University of Stellenbosch, Stellenbosch, South Africa

K. von Leipzig et al. (eds.), *Smart, Sustainable Manufacturing in an Ever-Changing World*, Lecture Notes in Production Engineering,
https://doi.org/10.1007/978-3-031-15602-1_63

1 Introduction

Cemented carbides are considered a workhorse material for a wide range of manufacturing industries. They are metal matrix composites (MMC) where metallic carbides, such as WC or TiC, act as reinforcing particles inside a metallic alloy binder phase, typically Co- or Ni-based, which acts as the metal matrix [1, 2]. The carbides contribute to the hardness and wear resistance, while the binder provides toughness and counters the brittle nature of the carbides [1, 3]. Cemented carbides are traditionally produced through press and sinter techniques; typical products are cutting tool inserts and high wear forming tools, such as dies. They are well-suited to these applications as they possess an excellent combination of thermal stability, hardness, and toughness [1, 4].

Laser powder bed fusion (L-PBF), an additive manufacturing (AM) technology, provides a potential alternative to conventional subtractive manufacturing processes, by offering advantages in the reduction of production time and feasibility of manufacturing complex geometries [2, 3, 5]. Producing high quality L-PBF parts depends on the use of powder that has is suited for AM.

The aim of this study was to determine the link between standard powder metallurgy (PM) powder characteristics, novel powder spreadability parameters, and the as-built properties of L-PBF WC–Co ISO 504:1975 designated CNMA 120404 cutting tool inserts. For this study specifically, spray-dried WC–Co powders, with Co contents of 12 and 17 wt%, respectively, were evaluated.

2 Materials and Methods

2.1 Raw Materials

Two different commercially available, agglomerated, and sintered WC–Co powders, that are typically used for high velocity oxygen fuel (HVOF) coatings, were used in this study: Praxair 1342 VM (WC-12Co) and Kennametal JetKote 117 (WC-17Co). As L-PBF of WC–Co is still under development, there are no AM powders available commercially. For ease of reference the respective powders are referred to as WC-12Co and WC-17Co, respectively. Table 1 shows the chemical composition of these powders, as reported by the suppliers.

Table 1 Powder composition, as per supplier datasheet

Powder description	WC (wt%)	Co (wt%)	Other (wt%)
WC-12Co	82.5	11.72	5.77
WC-17Co	77.8	17	5.2

2.2 Methodology

Standard powder characterisation methods were used to evaluate the raw powders. These methods included apparent density and flow rate, measured according to ASTM standards B212 and B213. Particle morphology and size was determined through image analysis using a scanning electron microscope (SEM), with concomitant energy dispersive spectroscopy (EDS) used for elemental analysis. The particle size distribution was measured using the light scattering technique with a Micromeritics Saturn DigiSizer.

Spreadability metrics, powder bed spread density (PBD) and percentage coverage, were determined with the use of a custom designed powder spreadability rig [6] that replicates the powder spreading process of L-PBF. Both the WC-12Co and WC-17Co powders were used to print the CNMA cutting tool inserts on a Concept Laser M2 L-PBF machine. Two sets of inserts were produced from each powder keeping the laser power (190 W) and scan speed (550 mm/s) constant while varying the hatch spacing at two different levels (80 and 100 μm). The layer thickness and laser spot size were kept constant at 30 μm and ~50 μm, respectively. The parts were removed from the base plate with an Agie Charmilles CA20 wire electrical discharge machine (W-EDM).

The as-built inserts were prepared for analysis using standard metallographic procedures for WC–Co. Density was measured using the Archimedes principle. Porosity as well as grain size and microstructure were investigated using optical microscopy and SEM. The hardness of the inserts was measured using the Rockwell hardness scale A (HRA) testing with a load of 60 kgf for a hold time of 3 s. The cobalt content was measured with energy dispersive spectroscopy (EDS) on the SEM. The presence of visible defects was determined for each set of build parameters. Powder X-ray diffraction (XRD) was performed on a Bruker D2 Phaser instrument. The influence of the precursor powders was then related to the as-built material characteristics.

3 Results and Discussions

3.1 Initial Characterization

3.1.1 Particle Morphology and Size

Figure 1 shows SEM images of the WC-12Co and WC-17Co powders at two levels of magnification. Both powders show spherical particles that are the sintered agglomerates of WC grains fused together by Co; this is the typical morphology that is expected for HVOF WC–Co powders. The particles of the WC-17Co powder are slightly more elongated than those of the WC-12Co powder. Table 2 reports the powder particle size distribution (PSD), as determined through light scattering technique. The PSDs

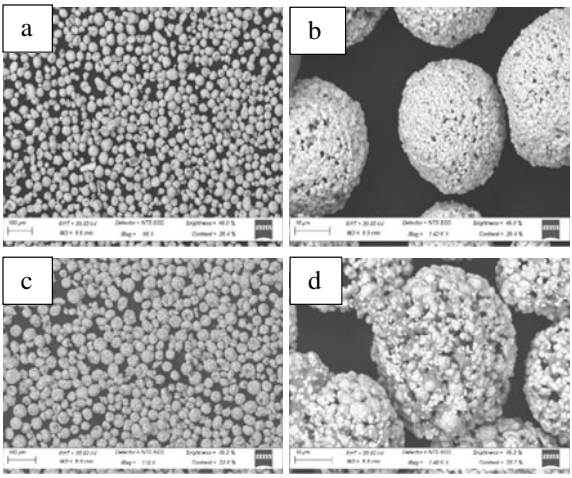

Fig. 1 SEM images of WC-12Co (**a**, **b**) and WC-17Co (**c**, **d**) with scale bars of 100 μm and 10 μm, respectively for (**a**, **b**) and (**c**, **d**)

Table 2 Powder particle size distributions

Powder designation	D10 (μm)	D50 (μm)	D90 (μm)
WC-12Co	21.50	31.94	43.05
WC-17Co	24.96	36.96	50.59

of both powders are similar, ranging from D10 around 20 μm to D90 around 50 μm. The WC-12Co powder is slightly smaller on the whole (around 13–14% across D10, D50 and D90) with a slightly narrower spread.

Elemental composition was determined by EDS spot analysis to identify WC grains and the Co regions that connect the WC grains. These features are indicated by the labels in Fig. 2, with WC showing lighter in colour than the darker grey Co regions. This visualizes the Co is the binder matrix while the WC grains are the reinforcing phase in the composite particles.

3.1.2 Powder Characteristics

The apparent density and flow rate for each powder are listed in Table 3. Each test was repeated three times, with the mean values along with the standard deviations reported. It is misleading to compare the apparent density values as the Co content of the two powders, and therefore the theoretical full density of the powder particles, differs. According to general relationships for full density WC–Co, a 12 wt% Co WC–Co material has a full density of 14.3 g/cm^3 while the density when the Co content is 17 wt% is 13.7 g/cm^3 [7]. By normalising the apparent density with the theoretical full density of each powder, the relative or fractional apparent density was calculated and is also reported in Table 3. As the relative density reflects the volume

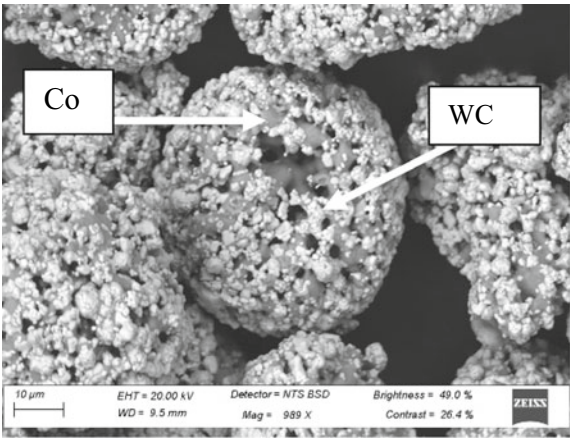

Fig. 2 SEM image of WC-17Co agglomerated powder particles with EDS spot analysis verification of WC and Co particles inside the agglomerates

Table 3 Powder properties—apparent density and flow rate

Powder	Apparent density (g/cm^3) {relative density}	Flow rate (s/50 g) {Volume powder/50 g (cm^3)}
WC-12Co	5.39 ± 0.01 {37.7%}	14.18 ± 0.98 {3.50}
WC-17Co	3.98 ± 0.00 {29.0%}	21.73 ± 0.53 {3.65}

fraction of actual material mass in a porous volume, the fractional porosity (volume % of air) is estimated as (1—relative density).

The WC-12Co powder has a higher relative apparent density than the WC-17Co powder; this indicates that the WC-12Co powder packs more densely, has less air gaps between powder particles, than the WC-17Co powder.

The implication of the higher full density of the WC-12Co on the flow rate can be partially explained by considering the volume of actual material that is occupied by the 50 g sample mass of each powder, also reported in Table 3. WC-12Co is denser, so the individual powder particles (without air gaps) occupy a smaller volume per unit mass. As the two powders have similar PSDs, the number of particles per unit mass of the WC-12Co is smaller than that of the WC-17Co powder and so the WC-12Co powder will take a shorter time to flow through the funnel. Nevertheless, the difference in volume per 50 g of powder is only 4%, while the difference in flow rate is 53%. Considering these two factors simultaneously indicates that the WC-17Co is more cohesive (more resistant to flow) than the WC-12Co powder.

3.1.3 Spreadability Metrics

The spreadability metrics, PBD and percentage coverage, are reported in Tables 4 and 5, respectively. The PBD was determined at layer heights of 60, 80 and 100 µm, while the percentage coverage was determined at layer heights of 40, 60 and 80 µm.

Table 4 Powder bed spread density (PBD)

Powder	Layer height (μm)		
	60	80	100
	PBD (g/cm^3) {relative density}		
WC-12Co	4.28 {29.9%}	4.51 {31.5%}	4.64 {32.5%}
WC-17Co	2.96 {21.6%}	2.52 {18.4%}	2.79 {20.4%}

Table 5 Percentage coverage (by area)

	Layer height (μm)		
	40	60	80
	Percentage coverage		
WC-12Co (%)	52	81	88
WC-17Co (%)	56	82	56

Both powders have a PBD lower than their apparent density (Table 3); however, the difference between the relative PBD and relative apparent density is larger, 7.4–10.6%, for the WC-17Co as compared to the WC-12Co powder, 5.2–7.8%. The implication of this result is that the reduction in packing density due to the action of spreading the powder across the baseplate is higher for the WC-17Co powder than the WC-12Co. This correlates with the flow rate result that indicates that the WC-17Co is more cohesive, more resistant to flow and spreading, than the WC-12Co powder. The elongated particle shape may have increased interparticle friction that may have affected the flowability. Similar results are presented by Snow et al. [8]. The larger particle sizes in WC-17Co would hinder spreadability at each layer height. This was observed by Cordova et al. [9] who also noted that large powder particles or agglomerates block the path for further powder spread. This creates lines or tracks across the base plate where little too no powder is present; these areas of low powder result in less material being spread across the base plate, resulting in a lower PBD.

For WC-12Co, there is a directly proportional relationship between percentage coverage and layer height. In contrast, the percentage coverage for WC-17Co increases as layer height increases from 40 to 60 μm, but then decreases substantially at a layer height of 80 μm. At least 10% of the particles in both powders are larger than the first layer height, 40 μm. This explains the low percentage coverage results at a layer height of 40 μm, as many particles would not fit under the gap between the base plate and re-coater blade and would be pushed across the plate instead of being deposited as a powder layer. Additionally, the more cohesive WC-17Co powder may form clumps or agglomerates of the composite particles, that are not broken up by the shear force of the re-coater blade moving across the baseplate when a higher layer height is used, such as is the case for the 80 μm layer height result. The result is that the percentage coverage drops after an optimal layer height is reached.

3.2 Post Printing Characterization

3.2.1 Prints and Defects

The prints were successfully performed. There were, however, issues with the WC-12Co inserts as many of them curled and warped off the base plate during the L-PBF process. This may be due to insufficient laser power, yet the parameters chosen were found to be the most beneficial to produce near defect-free components [10]. The final samples are shown in Fig. 3.

The physical properties of the inserts were measured and are tabulated in Table 6 [10]. It should be noted that even though WC-17Co powder had lower relative apparent density and relative PBD than WC-12Co, the as-built density of the final L-PBF inserts built of the WC-17Co was higher than the WC-12Co inserts. Another way of viewing this result is by considering that even though the loose WC-12Co powder packs more densely and spreads more densely than the WC-17Co powder, with less air gaps between powder particles, the residual level of porosity in the as-built inserts was higher for the WC-12Co inserts. This is a counter-intuitive result but it can be explained by considering the influence of the higher Co content. This is discussed in more detail after considering the implications of the hardness testing results.

The hardness measured for WC-17Co inserts was higher than that of the WC-12Co inserts. Two factors influence the hardness: the Co content and the residual porosity in the as-built material. Typically, a cemented carbide with a higher WC content and thus lower Co content, relates to a higher hardness [7]. A higher level of residual porosity

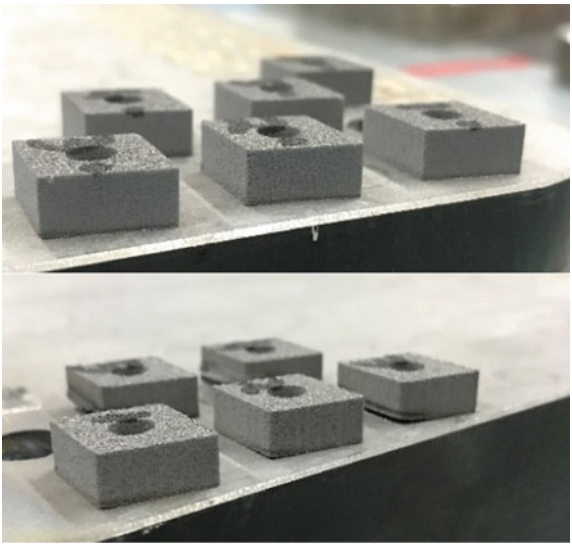

Fig. 3 Printed CNMA samples from (Top) WC-12Co and (Bottom) WC-17Co [10]

Table 6 CNMA insert properties

	WC-12Co		WC-17Co	
Hatch Spacing (μm)	80	100	80	100
Density [g/cm^3] (%)	12.48 (86.1)	12.32 (85.0)	12.84 (93.0)	12.59 (91.2)
Hardness [HRA]	53.2 ± 10.7	54.2 ± 9.6	57.3 ± 8.1	60.3 ± 3.2
wt% Co	9.45	9.99	16.32	16.67

correlates to a lower hardness. While the difference in Co content between WC-12Co and WC-17Co is 5 wt%, the corresponding difference in fractional Co volume is (26.5–19.3) = 7.2 vol.%. Additionally, EDS analysis of the inserts indicated that the final Co content of the WC-12Co inserts was <10 wt%, indicating that around 2 wt% Co evaporated during printing. In contrast, <1 wt% of Co evaporated during printing of the WC-17Co, as shown in Table 6. While the WC-17Co samples had a higher vol.% of Co, which should correspond to a lower hardness, their as-built residual porosity (1—relative as-built density) was lower. The additional Co allows for a more stable melt since a higher fractional volume of the powder forms a liquid phase (Co) when exposed to the laser; this results in less evaporation, and better wetting and densification of the microstructure during printing. Thus the influence of the higher Co content in WC-17Co has a significant effect on both the density and residual porosity. The effect of the residual porosity on the hardness of the final as-built material was more significant than the Co content, with the denser WC-17Co displaying a higher hardness, despite it having a higher Co content.

3.2.2 Phase Identification

Figures 4 and 5 show comparisons of XRD results for each powder, as well as their respective printed inserts. XRD identifies the crystalline phases present in a material. The results reveal that W_2C and other η-phases, although absent in the precursor powders, are observed in all the as-built inserts. The formation of the W_2C phase results from the heat generated by the L-PBF process. A greater quantity of W_2C was measured in the inserts with a lower hatch spacing (80 μm). These correlates to increased laser track overlap at a lower hatch spacing, which results in a higher temperature at the intersection point due to the higher energy input per unit area. It is known that W_2C and η-phases are brittle in nature and affect the mechanical properties of the final samples [5].

4 Conclusion

Two commercially available WC–Co powders with Co contents of 12 and 17 wt%, respectively, were evaluated for this investigation. The powders were evaluated

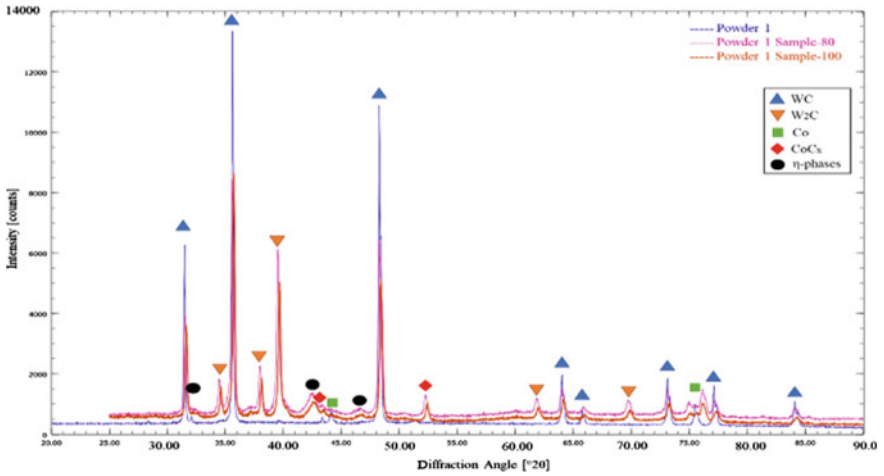

Fig. 4 X-Ray Diffraction phase analysis results for WC-12Co and printed insert samples from each hatch spacing

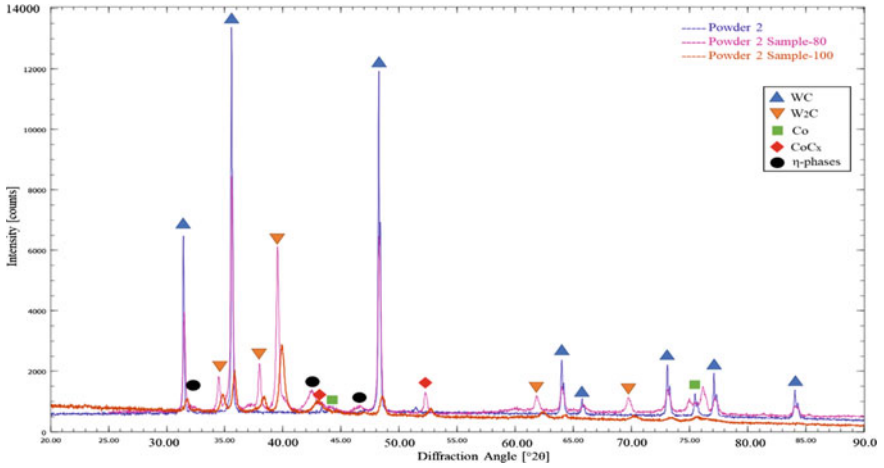

Fig. 5 X-Ray Diffraction phase analysis results for WC-17Co and printed insert samples from each hatch spacing

according to their powder characteristics: particle size and shape, apparent density, and flow rate, as well as the spreadability performance, as indicated by powder bed spread density and percentage coverage. The powders were then used to print CNMA inserts using L-PBF, which were then further characterised. The following conclusions are drawn from the results:

- The WC-12Co powder has primarily spherical particles whilst those of WC-17Co are slightly elongated. The particle sizes of the WC-12Co powder are slightly smaller.
- The WC-12Co powder has a higher apparent density than WC-17Co, which is partially due to its lower Co content. However, when considering the relative apparent density, it is clear that the WC-12Co powder packs more densely.
- The WC-12Co powder has a faster flow rate than WC-17Co. Both powders flowed freely, despite the more cohesive nature of the WC-17Co powder.
- The WC-12Co powder has better spreadability than WC-17Co, displaying both denser packing and a higher percentage coverage of the powder bed baseplate. It was observed that the percentage coverage increased as the layer height increased. This is attributed to its smaller particles and low cohesive forces as evident in the flow rate test. Both powders displayed poor spreadability at a 40 μm layer height as more than 10% of their powders are larger than 40 μm and are therefore dragged across the baseplate instead of being deposited.
- Inserts built from the WC-12Co powder warped off the base plate. Insufficient laser power, inadequate powder spreading in the case of WC-17Co, and the development of residual stress in the inserts may have contributed to this result.
- While the WC-17Co powder does not spread as well or pack as densely as the WC-12Co powder, the as-built density of the WC-17Co inserts is higher than the WC-12Co inserts. This is attributed to the higher Co content resulting in a more stable melt; this conceivably results in better printing behaviour contributing to denser parts.
- The as-built WC-17Co inserts measured higher hardness, even though a higher Co content was measured. This is attributed to the more significant influence of the residual porosity, that has a lower value for the WC-17Co inserts. The presence of the W_2C phase and η-phase also contributed to an increase in hardness.
- Printing parameters were seen to be optimal as components were successfully built with very little variation in Co wt% before and after printing.

Further experimentation is needed to quantify the relationship between powder characteristics, defects, and final build properties for L-PBF WC–Co. Various alloys could also be investigated to see similarities between powders investigated in this study and whether similar properties/defects are found post printing.

Acknowledgements The authors wish to acknowledge the financial support received from the Department of Science and Innovation and the National Research Foundation in South Africa (Grant Nos: 41292 and 129313). The opinions expressed and conclusions arrived at are those of the author/s and are not necessarily to be attributed to the Centre of Excellence in Strong Materials.

References

1. Schubert, W.D., Lasser, E., Bohlke, W.: Cemented Carbides—A Success Story, p. 2. International Tungsten Industry Association (2010)

2. Petersson, A.: Cemented Carbide Sintering: Constitutive Relations and Microstructural Evolution. KTH Materials Science and Engineering, Stockholm (2004)
3. Da Silva, A.G.P., Schubert, W.D., Lux, B.: The role of the binder phase in the WC-Co sintering. Mater. Res. **4**(2), 59–62 (2001)
4. Kumar, S.: Manufacturing of WC-Co moulds using SLS machine. J. Mat. Proc. Tech. **209**, 3840–3848 (2009)
5. Bricin, D., Kriz, A.: Processability of WC-Co powder mixtures using SLM additive technology. MM Sci. J., Czech Republic, pp. 2939–2945 (2019). https://doi.org/10.17973/MMSJ.2019_06_2018115
6. Parker, B.S., Blaine, D.C.: Blending of powders for in-situ alloying of Ti-6Al-4V laser powder bed fusion, MEng thesis, Stellenbosch University, South Africa, [unpublished] (2021)
7. Landolt-Börnstein, Properties of Hardmetals and Cermets, Group VIII. Springer Materials (2002)
8. Snow, Z., Martukanitz, R., Joshi, S.: On the development of powder spreadability metrics and feedstock requirements for powder bed fusion additive manufacturing. Addit. Manuf. **28**, 78–86 (2019)
9. Cordova, L., Bor, T., de Smith, M., Campos, M., Tinga, T.: Measuring the spreadability of pre-treated and moisturized powders for laser powder bed fusion. Addit. Manuf. **32**, 101082 (2020)
10. Hagedorn-Hansen, D.: Laser powder bed fusion of tungsten carbide cobalt cutting tools, Ph.D. thesis, Stellenbosch University, South Africa, [unpublished] (2021)

Preyin Govender obtained his Beng and M.Eng. degree in Mechanical Engineering from the Stellenbosch University. Currently, he is persuing his Ph.D. in Mechanical Engineering.

Devon Hagedorn-Hansen obtained his M.Eng. degree in Industrial Engineering from Stellenbosch University and has recently concluded his defence for his Ph.D. in Industrial Engineering. Devon is the founder and Managing Director of HH Industries.

Deborah Blaine is an Associate Professor of Mechanical and Mechatronics Engineering at Stellenbosch University. She is also the Ceramics Focus Area coordinator for the DSI-NRF CoE for Strong Materials.

Natasha Sacks is a Professor of Advanced Manufacturing at Stellenbosch University. Her research interests include materials science, and additive and subtractive manufacturing.